SAND2016-4046C

Radiative transfer modeling of surface chemical deposits

Thomas A. Reichardt* and Thomas J. Kulp
Sandia National Laboratories, P. O. Box 969, MS 9033, Livermore, CA, USA 94551

ABSTRACT

Remote detection of a surface-bound chemical relies on the recognition of a pattern, or "signature," that is distinct from the background. Such signatures are a function of a chemical's fundamental optical properties, but also depend upon its specific morphology. Importantly, the same chemical can exhibit vastly different signatures depending on the size of particles composing the deposit. We present a parameterized model to account for such morphological effects on surface-deposited chemical signatures. This model leverages computational tools developed within the planetary and atmospheric science communities, beginning with T-matrix and ray-tracing approaches for evaluating the scattering and extinction properties of individual particles based on their size and shape, and the complex refractive index of the material itself. These individual-particle properties then serve as input to the Ambartsumian invariant imbedding solution for the reflectance of a particulate surface composed of these particles. The inputs to the model include parameters associated with a functionalized form of the particle size distribution (PSD) as well as parameters associated with the particle packing density and surface roughness. The model is numerically inverted via Sandia's Dakota package, optimizing agreement between modeled and measured reflectance spectra, which we demonstrate on data acquired on five size-selected silica powders over the 4-16 μm wavelength range. Agreements between modeled and measured reflectance spectra are assessed, while the optimized PSDs resulting from the spectral fitting are then compared to PSD data acquired from independent particle size measurements.

Keywords: Particulate surface, reflectance, hyperspectral, chemical signature

1. INTRODUCTION

Interpreting reflectance spectra of particulate surfaces has long been of keen interest in the geological[1] and planetary[2] science communities, and is highly relevant for other sensing and security applications as well. For particulate surfaces, the reflectance spectrum depends upon the optical properties (i.e., the complex refractive index) of the chemicals composing the surface as well as morphological parameters of the surface itself. As a result, the same chemical can exhibit vastly different spectra, or "signatures," depending on the size of particles composing the deposit.[3,4] There is strong interest in understanding the impact of morphology on such chemical signatures, and in developing reflectance models which can compute signatures displaying behavior consistent with observed dependencies. Here we present such a model, which leverages computational tools developed within the planetary and atmospheric science communities for evaluating the scattering and extinction properties of individual particles based on their size and shape, and the complex refractive index $n+ik$ of the material itself. These individual-particle properties then serve as input to the solution for the reflectance of a particulate surface composed of these particles[5]. The inputs to the model include parameters associated with a functionalized form of the particle size distribution (PSD) as well as parameters associated with the particle packing density and surface roughness. The model is numerically inverted via Sandia's Dakota[6] package, optimizing agreement between modeled and measured reflectance spectra, which we demonstrate on data acquired on five size-selected silica powders over the 4-16 μm wavelength range.

*tareich@sandia.gov; phone 1 925 294-4776; fax 1 925 294-2338

2. BACKGROUND AND APPROACH

Crystalline quartz has been the subject of most prior comparisons of particulate-surface reflectance models to measurements over a broad range of wavelength and refractive index. An early such study was presented by Conel[7], who performed a radiative transfer analysis of crystalline quartz reflectance spectra. Moersch and Christensen[8] later compared the results of five different reflectance models to emissivity spectra acquired on size-selected quartz particles. The model producing the best agreement with data still performed poorly in regions of large k. Wald and Salisbury[9] added to these models a 100-stream doubling model, which performed better for coarser than finer particles. Mustard and Hayes[10] utilized a model similar to the best-performing model of Moersch and Christensen[8], focusing on the impact of hyperfine particles on their reflectance spectra of quartz. Pittman et al.[11] revisited the results of Moersch and Christensen[8], attempting to improve the match between measurements and model by applying corrections to the Mie scattering computations of the single-particle scattering and extinction properties.

While crystalline quartz thus has an established history in such studies, it is a birefringent material, necessitating that reflectance models average relevant computations over the ordinary and extraordinary values of the refractive index. In our initial assessment of the reflectance model, we avoid the complication associated with birefringent materials, and instead compare to infrared reflectance spectra acquired on non-birefringent fused silica (sometimes referred to as "fused quartz" in the literature) powders as reported by Kulp et al.[3], hereafter referred to as *ideal system* data for comparison to our modeling results. Infrared reflectance spectra of silica powders have been long known to display a strong dependence on particle-size[12], and the refractive index of silica has been well studied[13]. In addition, size-selected silica powders are commercially available; Table 1 lists the five size-specific samples used in this study.

Table 1. The five commercially available (from Washington Mills North Grafton, Inc.), size-selected silica powders used in this study.

MESH SIZE	NOMINAL SIZE RANGE
≥325	≤44 μm
≥200	≤74 μm
≥120	≤125 μm
100-200	74-149 μm
50-100	149-297 μm

Our reflectance model couples a rigorous radiative transfer solution (for a semi-infinite layer of well-separated particles), but with a simplified approximation for particle shape, and with phenomenological "patches" to account for packing density and surface roughness, allowing for the development of a parameterized model for the reflectance of a particulate surface. These patches, while necessary to extend a radiative transfer solution to packed particulate media, are not to be considered microphysically rigorous. We note that computational tools have been developed to provide rigorous microphysical assessments of electromagnetic radiation interacting with simplified particulate surface geometries (e.g., packed spheres[14]). However, natural particulate surfaces – even our silica-powder ideal systems – exhibit complexities in particle shape, packing arrangement, and surface geometry beyond which that have yet been considered with such numerical tools. At this point, the quantitative utility of our reflectance model is perhaps best demonstrated through model inversion, in which model-extracted parameters (e.g., the PSD) can be compared to independent measurements of physical properties. The work described here represents our initial effort to assess the reflectance model in such a manner.

3. REFLECTANCE MODEL FOR A PARTICULATE SURFACE

3.1 Deriving Surface Reflectance from Particle Scattering/Extinction Properties: The Ambartsumian Invariant Imbedding Solution

The reflectance of a particulate surface is related to the scattering and extinction properties of the particles composing that surface. To compute this relationship, we turn to the Ambartsumian nonlinear integral equation, an invariant

imbedding solution for a macroscopically flat, homogeneous, optically semi-infinite medium of dilute particles. It is derived via the principle of invariance: with the assumption an optically semi-infinite medium, the reflectance will remain unchanged upon the addition or removal of a plane layer of finite optical depth having the same optical properties as the original medium[15]. Mathematically removing this layer and setting the resulting change in reflectance to zero, and solving for the surface reflectance distribution function as a Fourier expansion in azimuth with coefficients R^m, results in[16,17,18]

$$\begin{aligned}(\mu+\mu_0)R^m(\mu,\mu_0) = {} & \frac{\varpi}{4}P^m(-\mu,\mu_0) \\ & + \frac{\varpi}{2}\mu_0\int_0^1 P^m(\mu,\mu')\,R^m(\mu',\mu_0)\,d\mu' \\ & + \frac{\varpi}{2}\mu\int_0^1 R^m(\mu,\mu')\,P^m(\mu',\mu_0)\,d\mu' \\ & + \varpi\mu\mu_0\int_0^1\int_0^1 R^m(\mu,\mu')\,P^m(-\mu',\mu'') \\ & \qquad \cdot R^m(\mu'',\mu_0)\,d\mu'\,d\mu'',\end{aligned} \tag{1}$$

where μ_0 is the absolute value of the cosine of the incident angle, μ is the absolute value of the cosine of the observation angle, ϖ is the single-scattering albedo, and P^m are the Fourier coefficients of the particle scattering function. An iterative solution of Eq. (1) is presented by Mishchenko et al.[5], and is available on the NASA GISS website[19]. For comparison to our ideal system data, the desired computational output is the plane albedo (i.e., the directional, hemispherical albedo), which is calculated from the R^0 coefficients as[5]

$$\text{Plane albedo}(\mu_0) = 2\int_0^1 R^0(\mu,\mu_0)\mu\,d\mu\,. \tag{2}$$

3.2 Parameterizing the Particle Shape and Size Distributions

Importantly, both the P^m coefficients and the value of ϖ in Eq. (1) are computed by averaging over particle populations. In our modeling of the silica powders, only one (non-birefringent) material is included, but averaging still occurs over the distributions of particle size and shape in the computation of the P^m and ϖ.

As presented by Kulp et al.[3], the particulates of silica powders are of complex geometries. With the intent of capturing the impact of shape and size on reflectance spectra, we consider a simplified spheroidal geometry, assuming the range of particle elongation can be represented by a single value. We then divide the population of particles equally between oblate and prolate spheroids of this elongation.

For the PSD, we use the bimodal volume log-normal distribution presented by Mishchenko et al.[20]

$$n(r) = \text{constant}\times r^{-4}\left\{\exp\left[-\frac{(\ln r-\ln r_{g1})^2}{2\ln^2\sigma_{g1}}\right]+\gamma\cdot\exp\left[-\frac{(\ln r-\ln r_{g2})^2}{2\ln^2\sigma_{g2}}\right]\right\}. \tag{3}$$

This distribution allows for two size modes, each of characteristic mean and width, which can vary independently of each other. The r_g and σ_g parameters represent the characteristic particle radius and width of each mode, respectively, while γ characterizes the population ratio between the two modes.

3.3 Computing Particle Scattering/Extinction Properties

We calculate the scattering phase function and single-scattering albedo through two methods. For smaller particles, we use the T-matrix for spheroids[21,22], where the expansion coefficients for the scattered field are related to those of the incident field. For larger particles, we use a Monte Carlo ray-tracing code[23,24], which launches multiple light rays at various positions, and considers multiple particle orientations as well.

3.4 Accounting for Packing Density

Defining the reflectance properties of a medium by the isolated scattering and extinction properties of individual particles is strictly applicable only for dilute media, for which the packing density does not exceed ~1%. If sufficiently

dilute, we can consider the scattering and extinction properties of the particles independently of each other. However, when the particles increase in packing density, their scattering and extinction properties are no longer independent. We invoke the static structure factor (SSF) to correct the scattering cross section and phase function for particle packing density. The SSF functions as a multiplier to the scattering phase function, and an analytical solution[25] is available for monodisperse spheres, which depends only on the fill factor f_{SSF}, the particle size parameter, and the scattering angle. We incorporate this factor into the model, calculating the SSF for a PSD-averaged volume-equivalent sphere.

There is also a need to account for the impact of packing density on the first-surface reflectance. An increase of the packing density has been observed to result in spectral features similar to those of a Fresnel reflection.[26] Related to this, Fresnel reflections have previously been incorporated into radiative transfer simulations of absorbing and scattering media.[27] We treat the interface as a fractional area F_{Fresnel}, of refractive index $n+ik$, with reflectance R_{Fresnel}. Electromagnetic radiation transmitted through this interface then interacts with the medium of reflectance R_{medium}, resulting in a total reflectance that sums these two contributions,

$$R = F_{\text{Fresnel}} \times R_{\text{Fresnel}} + \left(1 - F_{\text{Fresnel}} \times R_{\text{Fresnel}}\right) \times R_{\text{medium}} . \quad (4)$$

3.5 Accounting for Surface Roughness

The Ambartumian solution assumes a macroscopically flat surface. To account for macroscopic surface roughness, we allow for a variable incident angle $\theta_{0,\text{eff}}$.[28,29,30]

3.6 Model Summary

The reflectance model allows as many as nine variable parameters, one for the typical aspect ratio, five for the particle size distribution, one for the packing density for particles within the medium, one for the impact of packing density for particles on the surface, and the final one dealing with surface roughness. These nine parameters are summarized in Table 2.

Table 2. Reflectance model parameters and descriptions.

PARAMETER	DESCRIPTION
AR	Aspect ratio of spheroidal particles
r_{g1}	Particle radius parameter for coarse mode of bimodal PSD (μm)
σ_{g1}	Width parameter for coarse mode of bimodal PSD (μm)
r_{g2}	Particle radius parameter for fine mode of bimodal PSD (μm)
σ_{g2}	Width parameter for fine mode of bimodal PSD (μm)
γ	Ratio between fine and coarse modes of the bimodal PSD
f_{SSF}	Particle packing density for computing the SSF
F_{Fresnel}	Fill fraction of the Fresnel surface reflection
$\theta_{0,\text{eff}}$	Effective incidence angle to account for surface roughness (deg)

4. OPTIMIZING MODELING RESULTS TO MEASUREMENTS: MODEL INVERSION

Sandia's Dakota is used to optimize modeling results to measurements with the *nl2sol* solver, which uses a trust-region method to determine optimized parameters via forward difference calculations. We discretize the 4-16 um spectral range at 0.1-μm increments, resulting in 121 separate λ-dependent computations, and then divide those calculations over 64 processors. The specific values of n and k used for these computations, interpolated from the tabular values presented by Zolotarev[31], are presented in Fig. 1.

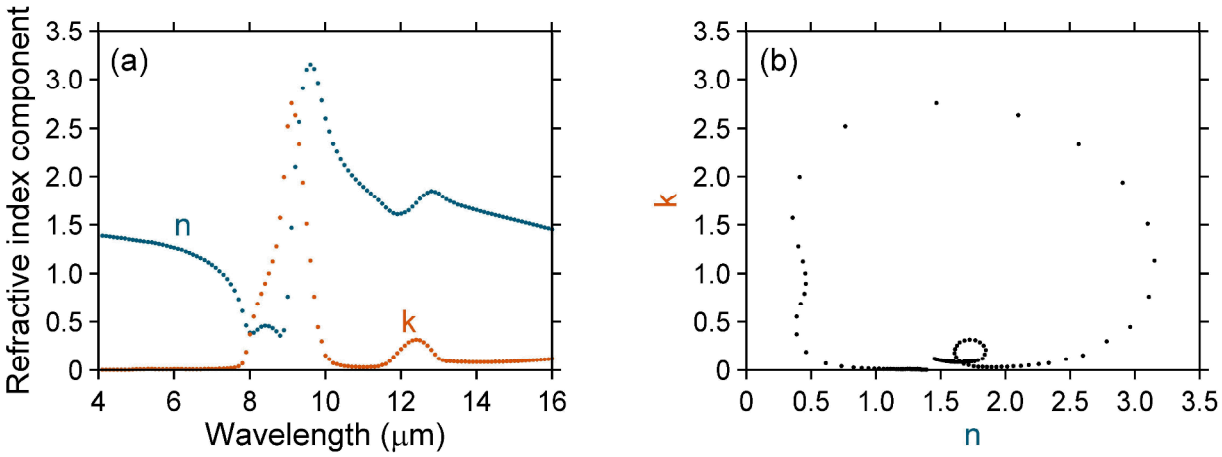

Figure 1. The 121-discrete refractive index *n*- and *k*-values for computing reflectance spectra of silica, plotted (a) as a function of wavelength and (b) versus each other.

Figure 2 displays optimized modeling results compared to measured spectra for the five silica powders. The root-mean-square difference between the optimized modeling results and the measurements is ~1% reflectance for all five powders. Moreover, the model captures the variability of reflectance with particle size, including the high-*k* Reststrahlen feature at ~9 μm, the amplitude of which increases by a factor of ~3 as the size-selected powders transition from the smallest to the largest particle sizes. The model also captures the behavior of the low-*k* features, <7 μm, and 10-12 μm, which both decrease significantly with increasing particle size. Such dependences of the reflectance on *n* and *k* are discussed in detail by Moersch and Christensen[8].

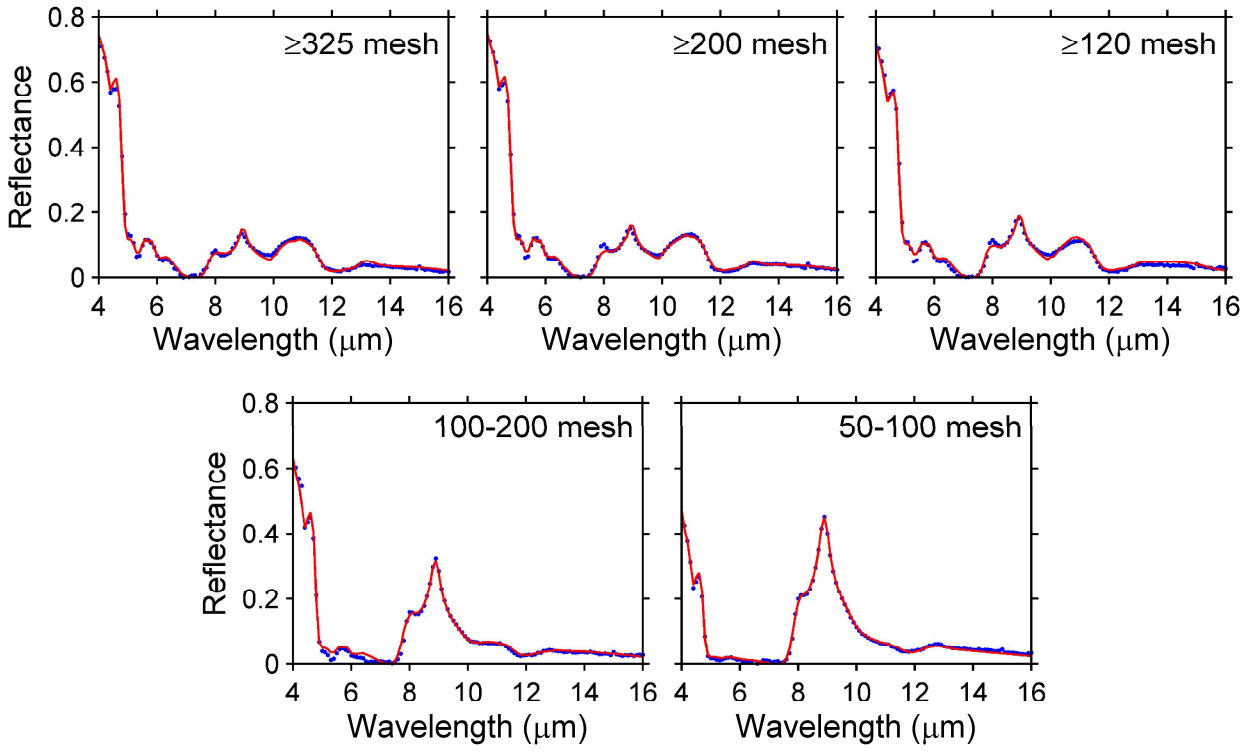

Figure 2. Measured (blue) and modeled (red) reflectance spectra of the five silica powders.

The results displayed in Fig. 2 demonstrate the agreement that can be achieved between modeled and measured reflectance spectra. However, considering the number of parameters that are allowed to vary in achieving this agreement, as well as the phenomenological "patches" required to account for packing density and surface roughness, a resulting concern is that the ideal system data are potentially being over-fit by the model. Addressing this concern, Fig. 3 provides a comparison between the PSDs determined by the optimized spectra in Fig. 2 and those measured via laser diffraction, as described by Kulp et al.[3] With perhaps the exception of the ≥200 mesh, the PSDs extracted from fitting the reflectance spectra display good qualitative agreement with laser-diffraction measurements. This agreement between reflectance-model-extracted PSDs and measured PSDs provides supporting evidence that the model is indeed quantitatively relating the particle size to its impact on reflectance spectra.

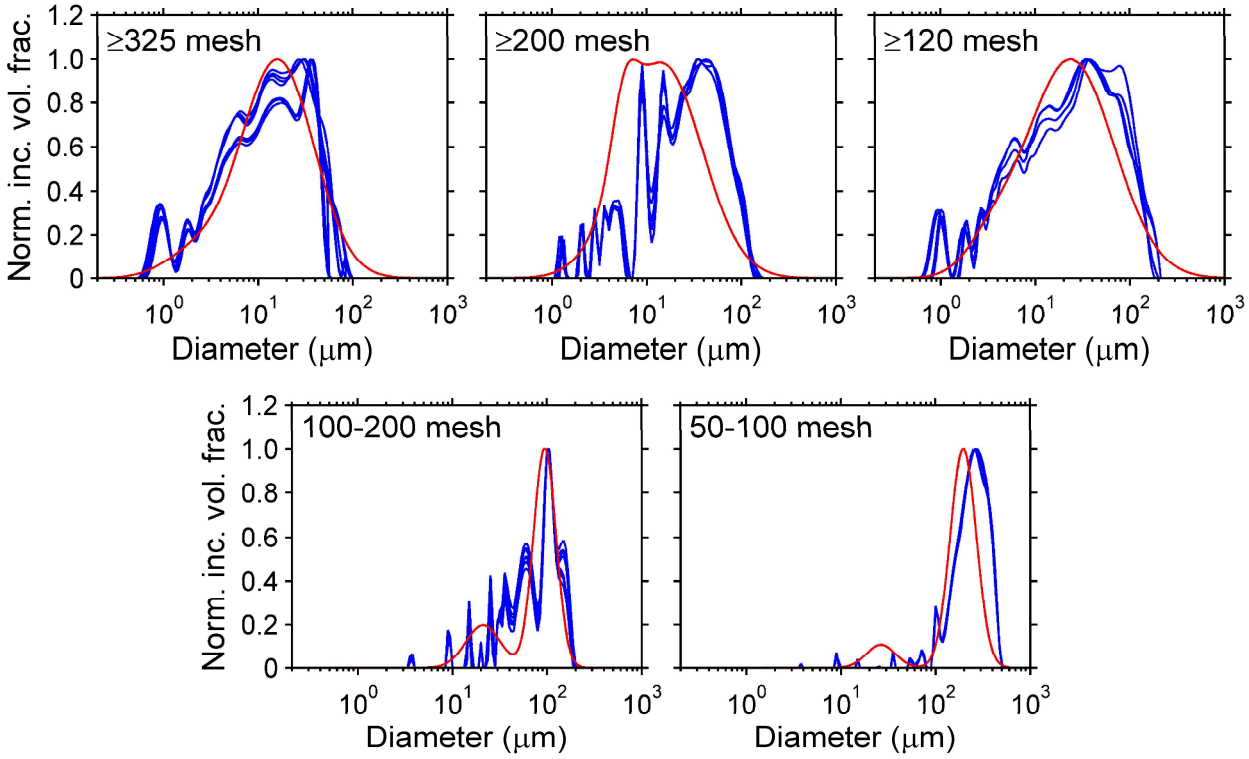

Figure 3. PSDs for the five silica powders, measured by laser diffraction (blue) and extracted from the optimized modeled infrared reflectance spectra (red). Multiple laser-diffraction results are included to provide some indication of measurement repeatability for each powder.

5. SUMMARY AND FUTURE WORK

A parameterized reflectance model has been presented which, when optimized, demonstrates agreement with measured reflectance spectra of silica powders. Furthermore, the PSDs extracted from the optimized spectra demonstrate agreement with PSDs measured via laser diffraction. Assessing the five size-selected silica powders over the 4-16-μm wavelength region provided a range of values for the imaginary component of the refractive index (7×10^{-5} – 2.8) and particle size (1- 300 μm) intended to challenge the model. Nevertheless, this work represents only an initial, limited test of the model. Given the approximations made in computing particle scattering/extinction properties, and especially the phenomenological "patches" to account for the impact of packing density and surface roughness, more rigorous tests are being pursued. Specifically, we will be narrowing the PSDs by size-selecting the silica powders to remove the fine-particle mode, and assessing if the extracted parameter γ follows suit. We also plan to vary the particle packing density, likely by pluviation[32], and to assess the resulting impact on f_{SSF} and $F_{Fresnel}$. An analogous study of the surface roughness parameter $\theta_{0,eff}$ will be conducted as well. In parallel with testing the model against systems designed specifically to

challenge its physical approximations, we will be assessing the model numerically as well, and calibration efforts are currently underway.[33]

ACKOWLEDGMENTS

The research described in this paper was supported by the U.S. Department of Energy (DOE) National Nuclear Security Administration (NNSA) Office on Nonproliferation and Verification Research and Development (DNN R&D). We gratefully acknowledge the guidance provided by Michael Mishchenko (NASA Goddard Institute for Space Studies, New York) at various stages of this work, as well as the advice provided by Patty Hough (Sandia National Laboratories, California) on parallel computing and the use of Dakota for optimization. Sandia is a multi-program laboratory operated by Sandia Corporation, a wholly owned subsidiary of Lockheed Martin Company, for the U.S. Department of Energy's National Nuclear Security Administration under contract DE-AC04-94AL85000.

REFERENCES

[1] van der Meer, F. D., van der Werff, H. M. A., van Ruitenbeek, F. J. A., Hecker, C. A., Bakker, W. H., Noomen, M. F., van der Meijde, M., Carranza, E. J. M., de Smith, J. B., and Woldai, T., "Multi- and hyperspectral geologic remote sensing: A review," International Journal of Applied Earth Observation and Geoinformation 14(1), 112-128 (2012).

[2] Singer, R. B., McCord, T. B., Clark, R. N., Adams, J. B., and Huguenin, R. L., "Mars surface composition from reflectance spectroscopy: A summary," J. Geophys. Res. 84(B14), 8415-8426 (1979).

[3] Kulp, T. J., Sommers, R. L., Murtagh, D., Krafcik, K. L., Mills, B. E., Reichardt, T. A., LaCasse, C. F., Fuerschbach, K. H., Craven-Jones, J., "Ideal system morphology and reflectivity measurements for model development and validation," Proc. SPIE 9840-16 (2016).

[4] Beiswenger, T. N., Myers, T. L., Brauer, C. S., Su, Y.-F., Blake, T. A., Ertel, A. B., Tonkyn, R. G., Szecsody, J. E., Johnson, T. J., Smith, M. O., and Lanker, C. L., "Experimental effects on IR reflectance spectra: particle size and packing," Proc. SPIE 9840-17 (2016).

[5] Mishchenko, M. I., Dlugach, J. M., Yanovitskij, E. G., and Zakharova, N. T., "Bidirectional reflectance of flat, optically thick particulate layers: an efficient radiative transfer solution and applications to snow and soil surfaces," J. Quant. Spectrosc. Radiat. Trans. 63, 409-432 (1999).

[6] Adams, B. M., Ebeida, M. S., Eldred, M. S., Jakeman, J. D., Swiler, L. P., Stephens, J. A., Vigil, D. M., Wildey, T. M., Bohnhoff, W. J., Dalbey, K. R., Eddy, J. P., Hu, K. T., Bauman, L. E., and Hough, P. D., "Dakota, A Multilevel Parallel Object-Oriented Framework for Design Optimization, Parameter Estimation, Uncertainty Quantification, and Sensitivity Analysis: Version 6.0 User's Manual," Sandia Technical Report SAND2014-4633, July 2014. Updated August 5, 2014.

[7] Conel, J. E., "Infrared emissivities of silicates: Experimental results and a cloudy atmosphere model of spectral emission from condensed particulate mediums," J. Geophys. Res. 74, 1614-1634 (1969).

[8] Moersch, J. E., and Christensen, P. R., "Thermal emission from particulate surfaces: A comparison of scattering models with measured spectra," J. Geophys. Res. 100(E4), 7465-7477 (1995).

[9] Wald, A. E., and Salisbury, J. W., "Thermal infrared directional emissivity of powdered quartz," J. Geophys. Res. 100(B12), 24665-24675 (1995).

[10] Mustard, J. F., and Hays, J. E., "Effects of hyperfine particles on reflectance spectra from 0.3 to 25 μm," Icarus 125, 145-163 (1997).

[11] Pitman, K. M., Wolff, M. J., and Clayton, G. C., "Application of modern radiative transfer tools to model laboratory quartz emissivity," J. Geophys. Res. 110, E08003 (2005).

[12] Hovis, W. A., and Callahan, W. R., "Infrared reflectance spectra of igneous rocks, tuffs, and red sandstone from 0.5 to 22 μm," J. Opt. Soc. Am. 56(5), 639-643 (1966).

[13] Kitamura, R., Pilon, L., and Jonasz, M., "Optical constants of silica glass from extreme ultraviolet to far infrared at near room temperature," Appl. Opt. 46(33) 8118-8133 (2007).

[14] Mackowski, D. W., and Mishchenko, M. I., "Direct simulation of extinction in a slab of spherical particles," J. Quant. Spectrosc. Radiat. Trans. 123, 103-112 (2013).

[15] Liou, K. N. [An Introduction to Atmospheric Radiation], 2nd edition, Academic Press, San Diego, pp. 277-279 (2002).
[16] Sobolev, V. V. [Light scattering in planetary atmospheres], trans. by W. M. Irvine, Pergamon Press, Oxford, Chapter 2 (1975).
[17] Dlugach, J. M, and Yanovitskij E. G., "The optical properties of Venus and the Jovian planets. II. Methods and results of calculations of the intensity of radiation diffusely reflected from semi-infinite homogeneous atmospheres," Icarus 22, 66-81 (1974).
[18] Yanovitskij, E. G., [Light scattering in inhomogeneous atmospheres], trans. by S. Ginsheimer and O. Yanovitskij, Springer, Berlin, Chapters 2 and 3 (1997).
[19] http://www.giss.nasa.gov/staff/mmishchenko/brf/
[20] Mishchenko, M. I., Travis, L. D., and Lacis, A. A. [Scattering, Absorption, and Emission of Light by Small Particles], Cambridge University Press, Cambridge, p. 161 (2002).
[21] Mishchenko, M. I., and Travis, L. D., "Capabilities and limitations of a current Fortran implementation of the T-matrix method for randomly oriented, rotationally symmetric scatterers," J. Quant. Spectrosc. Radiat. Trans. 60(3), 309-324 (1998).
[22] http://www.giss.nasa.gov/staff/mmishchenko/t_matrix.html
[23] Macke, A., and Mishchenko, M. I., "Applicability of regular particle shapes in light scattering calculations for atmospheric ice particles," Appl. Opt. 35(21), 4291-4296 (1996).
[24] http://tools.tropos.de/
[25] Mishchenko, M. I., "Asymmetry parameters of the phase function for densely packed scattering grains," J. Quant. Spectrosc. Radiat. Transfer 52(1), 95-110 (1994).
[26] Salisbury, J. W, and Wald, A., "The role of volume scattering in reducing spectral contrast of Reststrahlen bands in spectra of powdered minerals," Icarus 96, 121-128 (1992)
[27] Dombrovsky, L. A., Randrianalisoa, J. H., Lipiński, W., and Baillis, D., "Approximate analytical solution to normal emittance of semi-transparent layer of an absorbing, scattering, and refracting medium," J. Quant. Spectrosc. Rad. Trans. 112, 1987-1994 (2011).
[28] Shepard, M. K., Brackett, R. A., and Arvidson, R. E., "Self-affine (fractal) topography: Surface parameterization and radar scattering," J. Geophys. Res. 100, 11709-11718 (1995).
[29] Helfenstein, P. and Shepard, M. K., "Submillimeter-scale topography of the lunar regolith," Icarus 141, 107-131 (1999).
[30] Bandfield, J. L., Hayne, P. O., Williams, J.-P., Greenhagen, B. T., and Paige, D. A., "Lunar surface roughness derived from LRO Diviner Radiometer observations," Icarus 248, 357-372 (2015).
[31] Zolotarev, V. M., "Study of quartz glass by differential Fourier transform IR reflection spectroscopy: Bulk and surface properties," Optics and Spectrosc. 107(5), 754-767 (2009).
[32] Bachmann, C. M., Philpot, W., Abelev, A., and Korwan, D., "Phase angle dependence of sand density observable in hyperspectral reflectance," Rem. Sens. Environ. 150, 53-65 (2014).
[33] Engel, D., Hughes, M. S., Thompson, S. E., Reichardt, T. A., and Kulp, T. J., "Hierarchical multi-scale approach to validation and uncertainty quantification of hyper-spectral image modeling," Proc. SPIE 9840-22 (2016).